also to provide favored paths for ensuing extensile microcracks at the fault edges, within the subsurface Hertzian stress field. In the silicon carbide (Fig. 2), the shear faults form at the interfaces between the matrix grains and the grain boundary (YAG) phases. In the glass-ceramic (Fig. 4), they form at the mica-glass interface. This transition to apparent ductility in otherwise highly brittle ceramics is attributable to the large compressive component of contact stress fields (*13, 16*). The deflection of any downward propagating surface ring cracks along grain or interface boundaries away from the tensile stress trajectories (*13*) suppresses the development of a single cone crack, and at the same time, the action of strong shear stresses on the weak planes in the confining subsurface zone promotes the development of a population of highly stabilized microcracks. The latter kind of distributed damage has been widely considered in the fracture of rocks (*24*), where hydrostatic compressive fields are the norm, but not in advanced ceramics, whose design has hitherto been based predominantly on single-crack mechanics.

Our results are of special relevance to the mechanical response of ceramics where highly localized mechanical or thermal stresses are likely (*10*), such as in bearings, local impact conditions, refractories, and medical implants (for example, tooth restoratives). The implication is that one may design ceramic microstructures to change the very nature of the damage behavior and so optimize the mechanical response to suit particular applications.

REFERENCES AND NOTES

1. B. R. Lawn, *Fracture of Brittle Solids* (Cambridge Univ. Press, Cambridge, ed. 2, 1993).
2. P. L. Swanson, C. J. Fairbanks, B. R. Lawn, Y.-W. Mai, B. J. Hockey, *J. Am. Ceram. Soc.* **70**, 279 (1987).
3. P. L. Swanson, in *Fractography of Glasses and Ceramics*, V. Frechette and J. Varner, Eds., vol. 22 of *Advances in Ceramics* (American Ceramic Society, Columbus, OH, 1988), pp. 135–55.
4. B. R. Lawn, N. P. Padture, L. M. Braun, S. J. Bennison, *J. Am. Ceram. Soc.* **76**, 2235 (1993).
5. N. P. Padture, J. L. Runyan, S. J. Bennison, L. M. Braun, B. R. Lawn, *ibid.*, p. 2241.
6. P. Chantikul, S. J. Bennison, B. R. Lawn, *ibid.* **73**, 2419 (1990).
7. S.-J. Cho, B. J. Hockey, B. R. Lawn, S. J. Bennison, *ibid.* **72**, 1249 (1989).
8. S.-J. Cho, H. Moon, B. J. Hockey, S. M. Hsu, *Acta Metall.* **40**, 185 (1992).
9. F. Guiberteau, N. P. Padture, H. Cai, B. R. Lawn, *Philos. Mag. A* **68**, 1003 (1993).
10. K. L. Johnson, *Contact Mechanics* (Cambridge Univ. Press, London, 1985).
11. H. Hertz, *Hertz's Miscellaneous Papers* (Macmillan, London, 1896), chaps. 5 and 6.
12. F. C. Roesler, *Proc. Phys. Soc. London Sect. B* **69**, 981 (1956).
13. F. C. Frank and B. R. Lawn, *Proc. R. Soc. London Ser. A* **299**, 291 (1967).
14. F. B. Langitan and B. R. Lawn, *J. Appl. Phys.* **40**, 4009 (1969).
15. T. R. Wilshaw, *J. Phys. D* **4**, 1567 (1971).
16. B. R. Lawn and T. R. Wilshaw, *J. Mater. Sci.* **10**, 1049 (1975).
17. D. Tabor, *Hardness of Metals* (Clarendon, Oxford, United Kingdom, 1951).
18. T. O. Mulhearn, *J. Mech. Phys. Solids* **7**, 85 (1959).
19. Hexoloy SA, Carborundum, Niagara Falls, NY.
20. N. P. Padture, *J. Am. Ceram. Soc.* **77**, 519 (1994).
21. Macor, Corning, Inc., Corning, NY.
22. C. J. Fairbanks, B. R. Lawn, R. F. Cook, Y.-W. Mai, *Microstructure and the Strength of Ceramics*, vol. 8 of *Fracture Mechanics of Ceramics*, R. C. Bradt, A. G. Evans, D. P. H. Hasselman, F. F. Langes, Eds. (Plenum, New York, 1986), pp. 23–37.
23. K. Chyung, G. H. Beall, D. G. Grossman, in *Proceedings of 10th International Glass Congress*, M. Kunugi, M. Tashiro, N. Saga, Eds. (Ceramic Society of Japan, Tokyo, Japan, 1974), pp. 33–40.
24. J. C. Jaeger and N. G. W. Cook, *Fundamentals of Rock Mechanics* (Chapman & Hall, London, 1971).

25. Funding provided by the U.S. Air Force Office of Scientific Research. Financial support for F.G. from the Ministerio de Educación y Ciencia (DGICYT), Spain, is gratefully acknowledged.

19 November 1993; accepted 12 January 1994

Double Seismic Zone for Deep Earthquakes in the Izu-Bonin Subduction Zone

Takashi Iidaka and Yoshitsugu Furukawa

A double seismic zone for deep earthquakes was found in the Izu-Bonin region. An analysis of *SP*-converted phases confirms that the deep seismic zone consists of two layers separated by ~20 kilometers. Numerical modeling of the thermal structure implies that the hypocenters are located along isotherms of 500° to 550°C, which is consistent with the hypothesis that deep earthquakes result from the phase transition of metastable olivine to a high-pressure phase in the subducting slab.

The mechanism of deep earthquakes has been a puzzle since their discovery almost 70 years ago (*1, 2*) because the shear stresses necessary for ordinary brittle faulting reach impossibly high values at depths of several hundred kilometers. A range of mechanisms has been proposed for deep earthquakes, including plastic instabilities (*3, 4*), shear-induced melting (*5, 6*), and instabilities accompanying recrystallization (*7, 8*) or polymorphic phase transformation (*9–11*). As an explanation of deep events (*10*), each of these proposed mechanisms has been shown to suffer from certain inherent flaws.

Recent mineralogical experiments suggest that the occurrence of deep earthquakes may be related to a phase change of metastable olivine (*10–12*) to a high-pressure phase. Evidence for the presence of metastable olivine in subducting slabs has been found (*13, 14*) in the Izu-Bonin and Japan subduction zones. Transformational faulting within a metastable olivine wedge should produce a double seismic zone in the slab, because olivine above and below the wedge will warm and transform into spinel, whereas the colder interior material will remain untransformed.

The presence of a double seismic zone at depths of about 400 km in the Tonga region has been inferred on the basis of relocating hypocenters with the use of *P*, *pP*, and *PKP* arrivals (*15*). A schematic model for the occurrence of deep earthquakes in Tonga was proposed from seismicity and focal mechanism solutions. The Tonga double zone could be explained by bending, but a second observation, along with the observations of the converted phase from what may be the top of the slab, provides a more convincing case.

The existence of only a few seismic stations above these deep earthquakes limited improvement in the resolution of the relocated hypocenters. In addition, the lack of precise knowledge of the relation between the locations of deep earthquakes and the temperature structure of the slab prevents resolution of the cause of deep earthquakes. Here, we establish (i) the presence of a double seismic zone of deep earthquakes in the Izu-Bonin subduction zone, the same region where seismological evidence for the existence of a metastable zone within the slab was previously proposed (*13*) and (ii) the precise relation between the location of deep earthquakes and the temperature structure of the slab on the basis of $S - P$ converted wave analyses.

The Izu-Bonin region is one of the best areas to investigate the locations of deep earthquakes and velocity structure within the subducting slab, because there are many seismic stations in Japan that lie above the region where the slab is at depths of 100 to 450 km. We analyzed $S - P$ converted waves at the upper boundary of the slab to determine epicenters of the deep earthquakes relative to the upper plate boundary. The path of the converted wave is almost perpendicular to the upper boundary of the slab. The differential arrival times of the converted wave and the *P* wave are related to the distance between the focus of the earthquake and the upper boundary of the slab. We compared the location of the deep

T. Iidaka, Earthquake Research Institute, University of Tokyo, Yayoi 1-1-1, Bunkyo, Tokyo, Japan.
Y. Furukawa, Department of Geology and Mineralogy, Faculty of Science, Kyoto University, Kyoto, Japan.

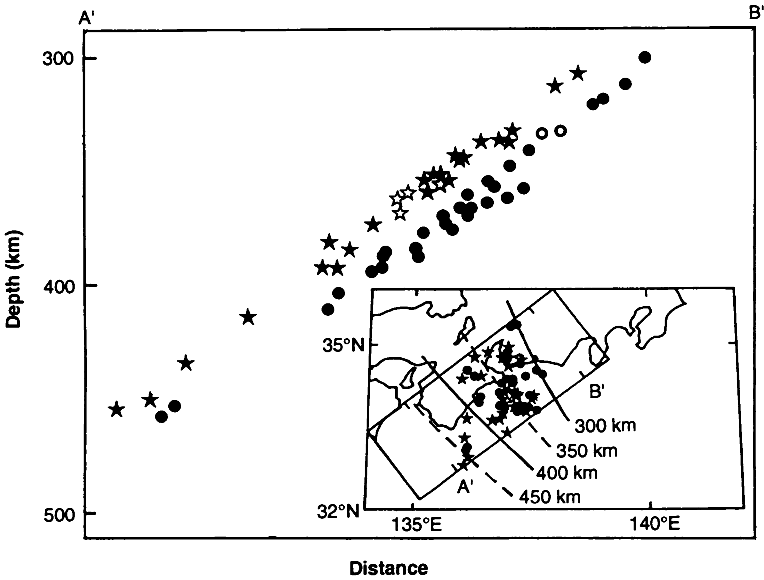

Fig. 1. Vertical cross section of deep earthquake hypocenters determined by the ISC. The earthquakes that show the converted phases are denoted by open symbols. A map of epicenters with lines of constant depth is shown in the inset. Different symbols are used for the upper (stars) and lower (circles) seismic zones to negate the possibility of artificial results caused by regional variations of the slab's dip angle.

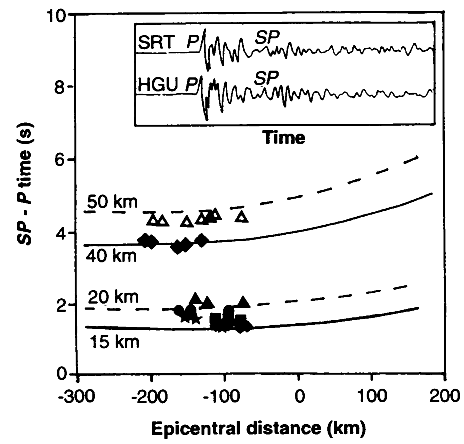

Fig. 3. Theoretical and observed data of *SP* – *P* time. Examples of the wave forms are shown in the inset. Different symbols are used for different earthquakes. The distance between the earthquake and the upper boundary of the slab is indicated. In the ray calculation, the velocity structures of the subducting Pacific slab and the surrounding mantle are assumed to be a heterogeneous slab model (*30*) and a modified Jeffreys-Bullen model with 3% slow velocities (*31*), respectively. V_P/V_S (velocity of *P* and *S* waves) = 1.73 is used.

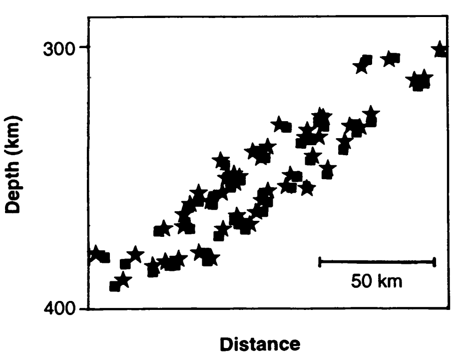

Fig. 2. Vertical cross section of relocated deep earthquakes, as shown by the iasp91 model (*17*). Two data sets made up of *IP* and *P* and *IP*, *P*, and *IS* data are shown by solid squares and stars, respectively.

seismic zone with the temperature structure obtained by theoretical calculation.

Using the ISC (International Seismological Center) bulletin, we selected 60 deep earthquakes (depth ≥ 300 km) that occurred between 1 January 1983 and 31 December 1989 in the Izu-Bonin region with a body wave magnitude greater than 3.0 (Fig. 1). We relocated the ISC hypocenters by taking into account the high-velocity Pacific slab and low-velocity mantle wedge (*13, 16*) because of the high density of seismograph stations; the relocated hypocenters were close to the ISC hypocenters. The accuracy of the hypocenters decreases toward the south as the distance between the epicenters and the seismic network increases. A vertical cross section of the deep events within a width of about 180 km shows a double seismic zone, with two planes of activity in the subducting lithosphere extending depths of 300 to 400 km (Fig. 1). The two planes are separated by ~20 km.

We relocated the hypocenters shown in Fig. 1 using the iasp91 model (*17*). To reduce the possibility of misreading arrival-time data, we did not use travel-time data with emergent phases (e*P*, *S*, e*S*) for the hypocenter determination. We used instead two data sets of arrival-time data, one of impulsive *P* (I*P*) and *P* arrivals and the other of I*P*, *P*, and impulsive *S* (I*S*) arrivals. Vertical cross sections through the relocated seismicity for the two data sets are similar to that for the ISC locations. The deep double seismic zone is clearly shown in both of the data sets (Fig. 2).

To establish the location of the deep earthquakes within the slab, we used *S* – *P* converted phase data seismograms recorded by the Wakayama micro-earthquake observatory at the Earthquake Research Institute at the University of Tokyo. Several seismograms show a clear later phase on the vertical component (Fig. 3). This later phase has the following characteristics. (i) Its vertical components have the largest amplitudes. (ii) The phase is recorded at widely separated seismic stations with a similar delay after the *P* arrival for each earthquake. (iii) The apparent velocity of the phase is similar to that of the direct *P* wave. (iv) The dominant particle motion of the phase is in the east-west direction, which is parallel to the dip direction of the subducting Pacific plate.

In considering possible causes of the later phase, we took account of previous studies in the Japan region (*18–21*). The upper bound-

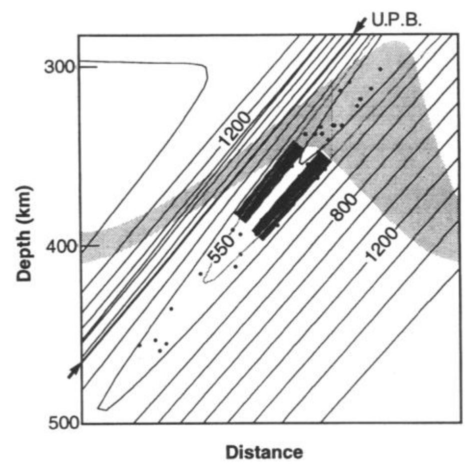

Fig. 4. Temperature structure of the subducting slab, with locations of deep earthquakes determined by the ISC. The upper plate boundary (U.P.B.) of the subducting Pacific slab is shown by the dark solid line (arrows). The α-β phase transition zone under equilibrium conditions is shown as a lightly hatched area (*25*). The clear double seismic zone (darkly shaded area) is shown along the isotherm of 550°C. In this calculation, a temperature- and pressure-dependent rheology are considered in the mantle wedge. The adiabatic temperature gradient is assumed to be 0.3 K km^{-1} (*32*), and the initial temperature structure of the oceanic lithosphere is calculated for the plate model (*33*). The age of the lithosphere and the subduction velocity in the direction perpendicular to the trench are taken to be 140 million years and 0.07 m $year^{-1}$, respectively (*34*). The temperature changes associated with phase transitions are not taken into account. The subduction angle in this region is set to be 50° on the basis of the seismicity.

ary of the subducting slab has a sharp boundary for wave conversions (*18–21*). As the characteristics of the later phase are consistent with those shown in previous studies (*19, 21, 22*), we confirm that the later phase is an $S - P$ converted wave at the upper boundary of the subducting Pacific slab (*21, 22*).

We estimated the distances between the sources and the upper boundary of the subducting slab from this $S - P$ converted phase data using a two-dimensional ray-tracing program (SEIS83) (*23*). The observed $SP - P$ time data show two populations, one of about 2 s and the other greater than 3 s (Fig. 3). These earthquakes with $SP - P$ times of either about 2 s or greater than 3 s are located in the upper seismic zone, at a distance of 15 to 20 km from the upper boundary of the slab, and in the lower seismic zone, at a distance of 40 to 50 km, respectively. This result is consistent with the hypocentral data shown in Figs. 1 and 2 and confirms that the deep seismic zone consists of two layers within the slab.

We calculated the temperature structure in the subducting lithosphere using a two-dimensional model (*24*) in which the rigid oceanic lithosphere is subducting under the arc and mantle flow is induced in the viscous mantle wedge. The calculated temperature structure in Fig. 4 shows that the double seismic zone, which is at depths of 340 to 400 km, is located below the transition zone from α-olivine to β-spinel (*25*). Moreover, the double seismic zone is parallel to the calculated 500° to 550°C isotherms in the subducting lithosphere as well as to the upper surface of the slab.

As shown in Fig. 4, the double seismic zone is located on the α-β phase transition zone and is parallel to the isotherms. These features are consistent with the hypothesis that deep earthquakes are triggered by a phase transition of the metastable olivine phase (*26, 27*) in the range of ~500° to 600°C; this temperature has been estimated to be about 600° to 700°C from experiments (*28*) and the kinetics of olivine-spinel phase transformation (*26, 29*). Seismicity in the Izu-Bonin region shows that the number of earthquakes increases at depths greater than about 300 km and decreases at depths greater than about 450 km. This depth range agrees with that of the metastable zone estimated by thermal modeling.

REFERENCES AND NOTES

1. H. H. Turner, *Mon. Not. R. Astron. Soc. Geophys. Suppl.* **1**, 1 (1922).
2. K. Wadati, *Geophys. Mag.* **1**, 162 (1928).
3. E. Orowan, *Geol. Soc. Am. Mem.* **79**, 323 (1960).
4. B. E. Hobbs and A. Ord, *J. Geophys. Res.* **93**, 10521 (1988).
5. D. T. Griggs, in *Nature of the Solid Earth*, E. C. Robertson, Ed. (McGraw Hill, New York, 1972), pp. 361–384.
6. D. T. Griggs and J. Handlin, *Geol. Soc. Am. Mem.* **79**, 347 (1960).
7. D. T. Griggs and D. W. Baker, in *Properties of Matter Under Unusual Conditions*, H. Mark and S. Frenback, Eds. (Wiley Interscience, New York, 1969).
8. M. Ogawa, *J. Geophys. Res.* **92**, 13801 (1987).
9. P. W. Bridgman, *Am. J. Sci.* **243A**, 90 (1945).
10. S. H. Kirby, *J. Geophys. Res.* **92**, 13789 (1987).
11. S. H. Kirby, W. B. Durham, L. A. Stern, *Science* **252**, 216 (1991).
12. H. W. Green II *et al.*, *Nature* **348**, 720 (1990).
13. T. Iidaka and D. Suetsugu, *ibid.* **356**, 593 (1992).
14. K. Suyehiro and T. Iidaka, in preparation.
15. D. A. Wiens, J. J. McGuire, P. J. Shore, *Nature* **364**, 790 (1993).
16. T. Utsu, *J. Phys. Earth* **23**, 367 (1975).
17. B. L. N. Kennett and E. R. Engdahl, *Geophys. J. Int.* **105**, 429 (1991).
18. I. Nakanishi *et al.*, *Geophys. J. R. Astron. Soc.* **67**, 615 (1981).
19. T. Matsuzawa *et al.*, *ibid.* **86**, 767 (1986).
20. K. Obara and H. Sato, *J. Geophys. Res.* **93**, 15037 (1988).
21. T. Iidaka, *Seismol. Soc. J.* **2**, 154 (abstr.) (1991).
22. J. Stefani *et al.*, *J. Geophys. Res.* **87**, 323 (1982).
23. V. Cerveny and I. Psencik, Program Package (SEIS83) (1983).
24. Y. Furukawa, *J. Geophys. Res.* **98**, 8309 (1993).
25. T. Katsura and E. Ito, *ibid.* **94**, 15663 (1989).
26. C. M. Sung and R. G. Burns, *Tectonophysics* **31**, 1 (1976).
27. L. Liu, *Phys. Earth Planet. Inter.* **32**, 226 (1983).
28. K. Suito, in *High-Pressure Research, Applications in Geophysics*, M. H. Marghnani and S. Akimoto, Eds. (Academic Press, New York, 1977), pp. 255–266.
29. D. C. Rubie *et al.*, *J. Geophys. Res.* **95**, 15829 (1990).
30. T. Iidaka *et al.*, *ibid.* **97**, 15307 (1992).
31. K. Suyehiro and I. S. Sacks, *Bull. Seismol. Soc. Am.* **67**, 1051 (1979).
32. R. Jeanloz and S. Morris, *Annu. Rev. Earth Planet. Sci.* **14**, 377 (1986).
33. B. Parsons and J. G. Sclater, *J. Geophys. Res.* **82**, 803 (1977).
34. R. D. Jarard, *Rev. Geophys.* **24**, 217 (1986).

35. Discussions with T. Lay and K. Suyehiro were helpful. We thank R. J. Geller for critically reading this manuscript. Partially supported by grants from the Japanese Ministry of Education, Science and Culture. We used the SEIS computer program of the Earthquake Research Institute.

23 September 1993; accepted 13 December 1993

Age of the Earliest Known Hominids in Java, Indonesia

C. C. Swisher III, G. H. Curtis, T. Jacob, A. G. Getty, A. Suprijo, Widiasmoro

$^{40}Ar/^{39}Ar$ laser-incremental heating of hornblende separated from pumice recovered at two hominid sites in Java, Indonesia, has yielded well-defined plateaus with weighted mean ages of 1.81 ± 0.04 and 1.66 ± 0.04 million years ago (Ma). The hominid fossils, a juvenile calvaria of *Pithecanthropus* and a partial face and cranial fragments of *Meganthropus*, commonly considered part of the Asian *Homo erectus* hypodigm, are at least 0.6 million years older than fossils referred to as *Homo erectus* (OH-9) from Olduvai Gorge, Tanzania, and comparable in age with the oldest Koobi Fora *Homo cf. erectus* (*Homo ergaster*) in Kenya. These ages lend further credence to the view that *Homo erectus* may have evolved outside of Africa. If the ancestor of *Homo erectus* ventured out of Africa before 1.8 Ma, the dispersal would have predated the advent of the Acheulean culture at 1.4 Ma, possibly explaining the absence of these characteristic stone cleavers and hand axes in East Asia.

The discovery in 1891 of a fossil hominid skull cap and femur in middle Pleistocene deposits exposed along the Solo River at Trinil, Java (Fig. 1), opened one of the most interesting chapters in the search for fossil hominids. At a time when little was known of our ancestors other than Neanderthal and Cro-Magnon man from Europe (*1*), Eugene Dubois set out from Holland to find Darwin's missing link. Dubois' remarkable discovery led him to propose a new species, *Anthropopithecus erectus*, which he subsequently referred to as *Pithecanthropus erectus* (*2*). Although Dubois himself later questioned the hominid affinities of his new species, subsequent work has placed the Trinil find within our own genus, renaming it *Homo erectus* (*3*).

By the mid-1900s, the central focus of hominid evolution shifted to the African continent, where the discovery of Pliocene fossil hominids and artifacts in direct association with datable volcanic rocks established Africa as the center for the origin of humans (*4*). In the 1960s and 1970s, the discovery of pre-Neanderthal hominids in Africa (*5–7*) and possibly Europe (*7*) referable to *H. erectus* sparked renewed interest in the type *H. erectus* of Java (*7–9*). In the Koobi Fora region of Kenya, specimen KNM-ER 3733 is now considered to have an age of slightly greater than 1.77 Ma, indicating that it represents perhaps the oldest hominid fossil referable as ancestral *H. erectus* (*7, 10*) (Fig. 2). The oldest stone "cleavers" and "hand axes," characteristic of the Acheulean culture, associated with Afri-

C. C. Swisher III and G. H. Curtis, Geochronology Center, Institute of Human Origins, 2453 Ridge Road, Berkeley, CA 94709, USA.
T. Jacob, A. Suprijo, Widiasmoro, Laboratory of Bio- and Paleoanthropology, Gadjah Mada University, Faculty of Medicine, Yogyakarta, Indonesia.
A. G. Getty, 50 California Suite, San Francisco, CA 94111, USA.